AGU PUBLICATIONS

Geophysical Research Letters

RESEARCH LETTER
10.1002/2014GL059400

Key Points:
- We model bimodal plasma sheet transport with bubbles in a realistic degree
- Bubble injections alter average magnetic field, entropy and FAC distributions
- Integrated effects of bubbles help resolve the pressure-balance inconsistency

Supporting Information:
- Readme
- movieS1
- movieS2

Correspondence to:
J. Yang,
jianyang@rice.edu

Citation:
Yang, J., R. A. Wolf, F. R. Toffoletto, S. Sazykin, and C.-P. Wang (2014), RCM-E simulation of bimodal transport in the plasma sheet, *Geophys. Res. Lett.*, *41*, doi:10.1002/2014GL059400.

Received 23 JAN 2014
Accepted 28 FEB 2014
Accepted article online 3 MAR 2014

RCM-E simulation of bimodal transport in the plasma sheet

Jian Yang[1], Richard A. Wolf[1], Frank R. Toffoletto[1], Stanislav Sazykin[1], and Chih-Ping Wang[2]

[1]Department of Physics and Astronomy, Rice University, Houston, Texas, USA, [2]Department of Atmospheric and Oceanic Sciences, University of California, Los Angeles, California, USA

Abstract Plasma sheet transport is bimodal, consisting of both large-scale adiabatic convection and intermittent bursty flows in both earthward and tailward directions. We present two comparison simulations with the Rice Convection Model—Equilibrium (RCM-E) to investigate how those high-speed flows affect the average configuration of the magnetosphere and its coupling to the ionosphere. One simulation represents pure large-scale slow-flow convection with time-independent boundary conditions; in addition to the background convection, the other simulation randomly imposes bubbles and blobs through the tailward boundary to a degree consistent with observed statistical properties of flows. Our results show that the bursty flows can significantly alter the magnetic and entropy profiles in the plasma sheet as well as the field-aligned current distributions in the ionosphere, bringing them into much better agreement with average observations.

1. Introduction

Plasma transport in the closed-field line region of Earth's magnetosphere was long thought to be dominated by large-scale sunward convection in the plasma sheet and gradient/curvature drift in the inner magnetosphere. Enforcing adiabatic drift of isotropic plasma in the plasma sheet implies that neglecting sources and losses, the flux tube partial entropy parameter $P_\lambda V^{5/3}$ is conserved along a drift path, where P_λ is the partial plasma pressure for particles with a given energy invariant λ and $V = \int ds/B$ is the flux tube volume. $PV^{5/3}$ is a fundamental parameter in the plasma sheet. Its gradient determines interchange instability [*Xing and Wolf*, 2007] and large-scale field-aligned currents (FACs). However, over the decades, the large-scale adiabatic convection picture has been confronted with challenges. *Erickson and Wolf* [1980] pointed out that the nearly uniform $PV^{5/3}$ distribution predicted by adiabatic drift theory significantly deviates from estimates made from empirical models, in which $PV^{5/3}$ has a strong and persistent tailward gradient through much of the plasma sheet [e.g., *Kaufmann et al.*, 2004; *Xing and Wolf*, 2007]. This is called the entropy inconsistency or the pressure-balance inconsistency [*Wolf et al.*, 2009]. Developing a unified theory that is consistent with the average observed tailward gradient of $PV^{5/3}$ is of vital importance for fully understanding plasma sheet transport, the physics of substorms, and magnetosphere-ionosphere coupling.

There is growing evidence that meso-scale processes, such as Bursty Bulk Flows (BBFs), are key elements in plasma sheet transport. They are estimated to account for 60%–100% of earthward transport of mass, energy, and flux [*Angelopoulos et al.*, 1994]. BBFs are also identified as plasma sheet bubbles, containing lower $PV^{5/3}$ than the background [e.g., *Pontius and Wolf*, 1990; *Sergeev et al.*, 1996]. The bubbles transport low entropy flux tubes to the near-Earth region through interchange, thus possibly resolving the entropy inconsistency. BBFs or bubbles are ubiquitous features of the plasma sheet, seen in substorm and non-substorm times, storm, and non-storm times. Studies also show that tailward flows are not rare [*Angelopoulos et al.*, 1999; *Guild et al.*, 2008]. The anti-sunward flows on the closed field lines are probably plasma sheet blobs with higher $PV^{5/3}$ than the background, the tailward-moving part of the vortex-like flows associated with bubbles [*Birn et al.*, 2004], or tailward bouncing of a bubble associated with interchange oscillations [*Wolf et al.*, 2012a]. Affected by those high-speed flows, the standard deviation of flow speed in the plasma sheet is several times larger than its mean value [*Angelopoulos et al.*, 1999]. The probability density function of plasma sheet flows suggests two components, long-duration slow flows and short-lived fast flows [*Borovsky et al.*, 1997; *Angelopoulos et al.*, 1999; *Guild et al.*, 2008].

Event studies of individual BBFs or bubbles and statistical analysis of their characteristic features have received much attention [e.g., *Hsu et al.*, 2012; *Runov et al.*, 2012]. However, their cumulative effects have not

been quantitatively determined. In this study, we aim to answer two questions: (1) What are the integrated effects of many localized bursty flows on average configuration of the plasma sheet and its coupling to the ionosphere? (2) To what extent do they help resolve the entropy/pressure-balance inconsistency?

2. RCM-E Results

The Rice Convection Model—Equilibrium (RCM-E) [*Toffoletto et al.*, 2003] strictly enforces the adiabatic drift condition, assuming that the pitch angle distribution is everywhere isotropic and that the associated energy invariant $\lambda = W_K V^{2/3}$ is conserved, where W_K is kinetic energy. The code also assumes that the distribution function $f(\lambda)$ is conserved along each drift path, except for the effects of electron precipitation and ion charge exchange. We use the high-resolution RCM-E to simulate two distinct cases: one that represents pure large-scale adiabatic slow convection and one that includes random bursty flows superposed on that background convection.

We model a hypothetical moderately enhanced convection interval with a 50 kV cross-polar-cap potential (CPCP) drop applied to the RCM simulation region, corresponding to Kp = 3. For initial conditions, both simulations use a T89 empirical magnetic field model (Kp = 1) [*Tsyganenko*, 1989] that is equilibrated with an empirical plasma pressure model [*Lemon et al.*, 2003]. The magnetic field is then reequilibrated every 5 min for both simulations. To model the large-scale slow-flow convection, $PV^{5/3}$ along the high-latitude boundary of RCM is adapted from the initial conditions $F(\phi)$ but scaled by a factor of a and kept time stationary as $PV^{5/3} = aF(\phi)$, where ϕ is the local time angle in the magnetosphere (0 at noon, π at midnight, and 0.5π and 1.5π at the dusk and dawn terminators). The constant $a = 1.1$ is designed to match $PV^{5/3}$ at the midnight boundary with the Kp = 3 condition. E_y along the high-latitude boundary is set as $-\frac{\mathrm{CPCP}}{2r}\cos(\phi)$, where r is the radial distance in the equatorial plane. Since the simulation without bursty flows starts to produce unphysical results after $T \sim 01{:}00$ when the magnetic field is extremely stretched in the magnetic transition region, we only study the first 55 min of this run.

To model intermittent bursty flows in the background convection, we assume that all the bubbles and blobs are created tailward of the RCM simulation region and are implemented through the nightside boundary. We design a disturbance in $PV^{5/3}$ to the background distribution in a form as

$$PV^{5/3}(\phi, t) = 1.5F(\phi)Max[0.005, 1 - dA_m(t)H(\phi)\cos(M\phi)] \tag{1}$$

Where

$$H(\phi) = \begin{cases} \cos^2(\phi - \pi) \ if \ |\phi - \pi| < \dfrac{\pi}{2} \\ 0 \qquad\quad if \ |\phi - \pi| \geq \dfrac{\pi}{2} \end{cases} \tag{2}$$

and

$$A_m(t) = \sum_{n=1}^{5} \cos\left(\frac{2\pi nt}{T} + 2\pi\zeta_{m,n}\right) \tag{3}$$

The factor 0.005 sets a floor to allow the maximum depletion to be 99.5%; d controls the degree of depletion/enhancement inside a bubble/blob; the coefficient 1.5 is designed to match the time-averaged $PV^{5/3}$ over the entire run with the empirical model (Kp = 3) right inside the midnight boundary at $X = -19$ R_E (see black and solid red lines in Figure 2a) and is determined by trial and error. $H(\phi)$ confines the disturbances to the nightside and to make them largest at midnight. Each bubble or blob channel has an angular width of π/M, where $M = 20$; therefore, the spatial scale for each bubble or blob in the dawn-dusk direction at ~20 R_E in the tail is comparable to the average size of bubbles in observations, i.e., $2 \sim 3$ R_E in the middle plasma sheet [*Nakamura et al.*, 2004]. $T = 2.5$ h is the length of the simulation. The time variation function $A_m(t)$ has a longest period T and shortest period $T/5$; $A_m(t)$ allows the enhancement or depletion in $PV^{5/3}$ to be as short as $T/10$ (half of the shortest period, i.e., 15 min), consistent with the time scales of characteristic durations of BBFs [Figures 8 and 9 of *Angelopoulos et al.*, 1994]. $\xi_{m,n}$ are random numbers to shift the phase of time variation for each channel m (from 1 to 20) and for each time period T/n. We also incorporate locally enhanced (or reduced) E_y for the bubbles (or blobs) to the background electric potentials on the boundary in a form as

$$E_y = -\frac{\mathrm{CPCP}}{2r}\cos(\phi) + cA_m(t)H(\phi)\cos(M\phi) \tag{4}$$

where the constant c controls the degree of enhancement and reduction. In order to represent the bursty flows in the plasma sheet to a realistic degree, we adjust the coefficients d in equation (1) and c in equation (4)

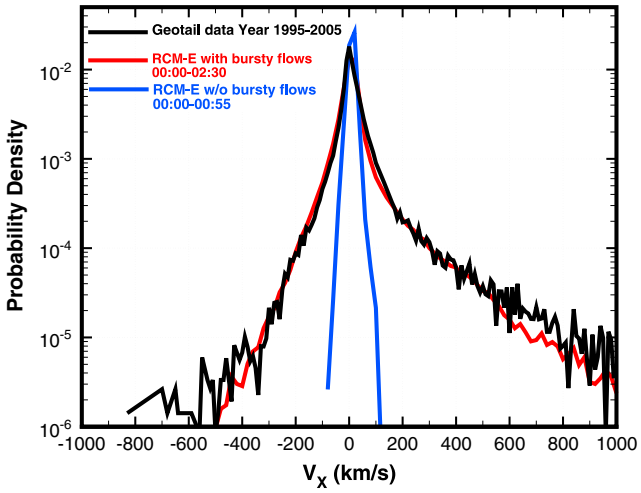

Figure 1. Probability density functions of V_X in the equatorial plane in Rice Convection Model—Equilibrium (RCM-E) simulations with (red) and without (blue) bursty flows, and from 11 years of Geotail data (black).

by trial and error to best match the probability density function obtained from Geotail observations (black line in Figure 1 below). For the simulation presented here, $d = 0.32$ and $c = 1.0$ mV/m.

Movie ms01 shows the $PV^{5/3}$ boundary conditions for the run with bursty flows. The highly localized depletion (enhancement) represents the imposed bubbles (blobs), although the $PV^{5/3}$ boundary condition is not really imposed when the flow is outward through the boundary. Movie ms02 presents an overview of results of this run, showing a dynamic picture of localized bursty flows in both earthward and tailward directions. Figure 1 compares the probability density functions (PDF) of V_X from Geotail data (in GSM) and RCM-E simulations. The selection criteria for the Geotail data are (1) $-19 < X < -10$ and $-10 < Y < 10$ Re, (2) plasma beta $\beta > 0.5$, (3) $B_Z/B_r > 0.5$, and (4) ion temperature $T_i > 1$ keV and ion number density $N_i < 1$ cm^{-3}. A total of 401,469 1 min-resolution Geotail V_X data are collected, from year 1995 to 2005. The velocities in the RCM-E are the sum of $\boldsymbol{E} \times \boldsymbol{B}$ and proton diamagnetic drift in the equatorial plane. Only ~0.13% data points have velocities greater than 1000 km/s in the simulation with bursty flows, but we only count the $|V_X| < 1000$ km/s data points in our statistical study. A total of 95,579 and 315,411 points are obtained for the same *X-Y* region as Geotail data in the simulation without bursty flows between $T = 00{:}00$ and 00:55 and with bursty flows between $T = 00{:}00$ and 02:30, respectively. By tuning the parameters *c* and *d*, we were able to make the calculated PDF in the simulation with bursty flows highly consistent with the Geotail data, with the probability of earthward flows higher than tailward. The standard deviation and the root mean square of V_X are ~5 times as large as the mean value (Table 1). However, the simulation without bursty flows shows very few points with the velocity magnitude higher than 100 km/s. The calculated standard deviation and the root mean square are comparable to its mean value. Table 1 also compares our results with other published data analysis, indicating that the simulation with bursty flows captures the basic flow statistical properties very well.

Figure 2 shows the plasma and magnetic field properties along the *x* axis. In the absence of bursty flows, the deviation of the $PV^{5/3}$ profile from the empirical model is substantial outside geosynchronous orbit (Figure 2a). If the model were able to handle the highly stretched configuration properly without producing strong numerical noise, $PV^{5/3}$ would become more flat in the plasma sheet at a later time, making the entropy inconsistency even more severe. The inconsistency is a result of enforced adiabatic convection of isotropic plasma in the RCM-E. For the case with BBFs, we take the 2.5 h averages as better approximations to the long-term statistical Tsyganenko models. The 2.5 h-average $PV^{5/3}$ has an approximately steady increase with radial distance outside 14 Re in the simulation with bursty flows, although it is still larger than the empirical model

Table 1. Statistical Flow Properties in the Central Plasma Sheet

	$<V_X>$ (km/s) (Mean)	$<(V_X - <V_X>)^2>^{1/2}$ (km/s) (Standard Deviation)	$<V_X^2>^{1/2}$ (km/s) (Root Mean Square)	*X* Range (Re)
RCM-E w/o bursty flows	10.8	12.9	16.9	−10 to −19
RCM-E with bursty flows	16.5	86.4	88.0	−10 to −19
Geotail data 1995–2005	26.5	93.8	97.5	−10 to −19
Borovsky et al. [1997]	N/A	N/A	75	~ −15 to −20
Angelopoulos et al. [1999]	20.5	82	84.5	~ −8 to −20
Guild et al. [2008]	16.1 ~ 18.9	88[a]	90[a]	~ −10 to −30

[a]Estimated from the black curve of Figure 4 in *Guild et al.* [2008]

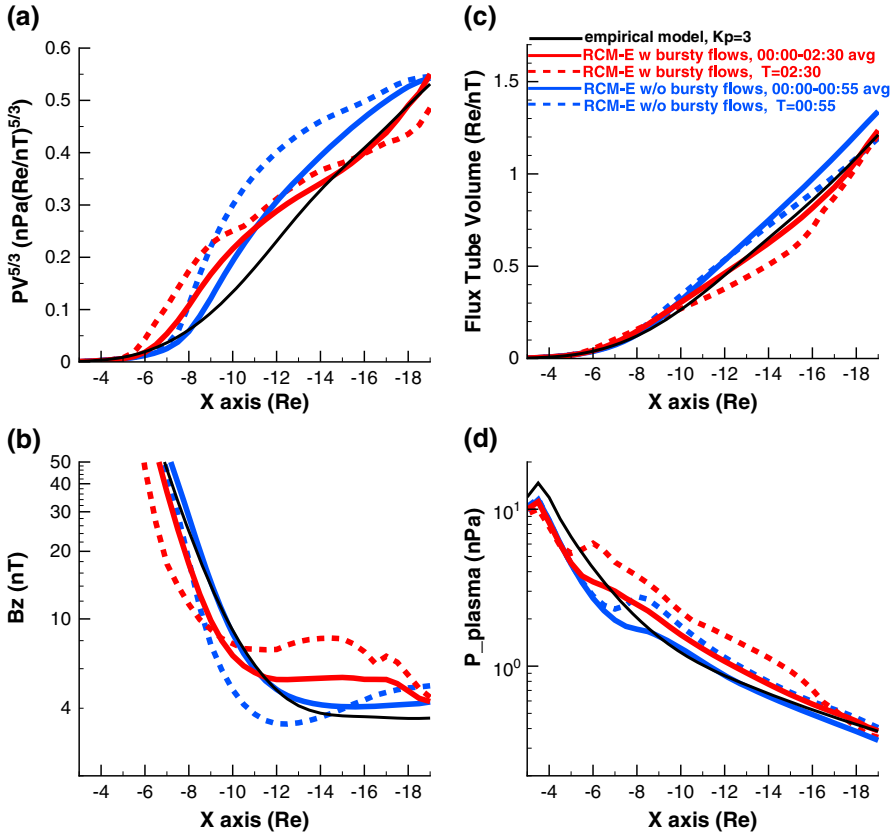

Figure 2. Key parameters along the *x* axis for an empirical model (black) and RCM-E simulations with (red) and without (blue) bursty flows.

from geosynchronous orbit to 14 R_E. The B_Z component in the simulation without bursty flows exhibits a profound minimum in the near-Earth plasma sheet (Figure 2b), and the reduction of B_Z at $X \sim -12$ R_E persists throughout the 55 min simulation, mimicking a substorm growth phase. Similarly, the inconsistency in B_Z between that simulation and the empirical model is also getting worse with simulation time. The simulation with bursty flows also yields more consistent time-average flux tube volume (Figure 2c) with the Kp = 3 model than that without bursty flows, while there is no clear change in the level of agreement on plasma pressure (Figure 2d).

Figure 3 shows the FAC densities in the ionosphere. The simulation with bursty flows at $T = 02{:}30$ shows numerous structures in the nightside auroral zone. They extend to as low as 60° latitude near local midnight. Some of those structures are clearly associated with bubbles and blobs, while some of them are associated with remnant $PV^{5/3}$ gradients from previous times. Besides those highly localized FAC patches, region 2 FACs can still be identified in the background, with upward current on the dawnside and downward current on the duskside. The time-average FAC density in Figures 3b and 3c clearly shows the main region 2 currents, with some localized FAC patches on the nightside. The time-average electric potentials in the ionosphere resemble the sunward convection part of the two cell potential pattern. Although the simulation without bursty flows shows the region 2 FACs as well, the pre-midnight downward region 2 currents are mostly confined in a thin band that is only ~ 1° thick with high peak intensity (Figures 3d–3f).

3. Discussion

The formalism of the RCM-E gives us the freedom to either allow or prohibit bubble injections through the tailward boundary, enabling us to adjust the boundary conditions of $PV^{5/3}$ and other characteristics to model two distinct modes of transport. It cannot be done easily either in models based on statistical observations or in global MHD simulations [e.g., *Guild et al.*, 2008]. Thus, the two RCM-E comparison

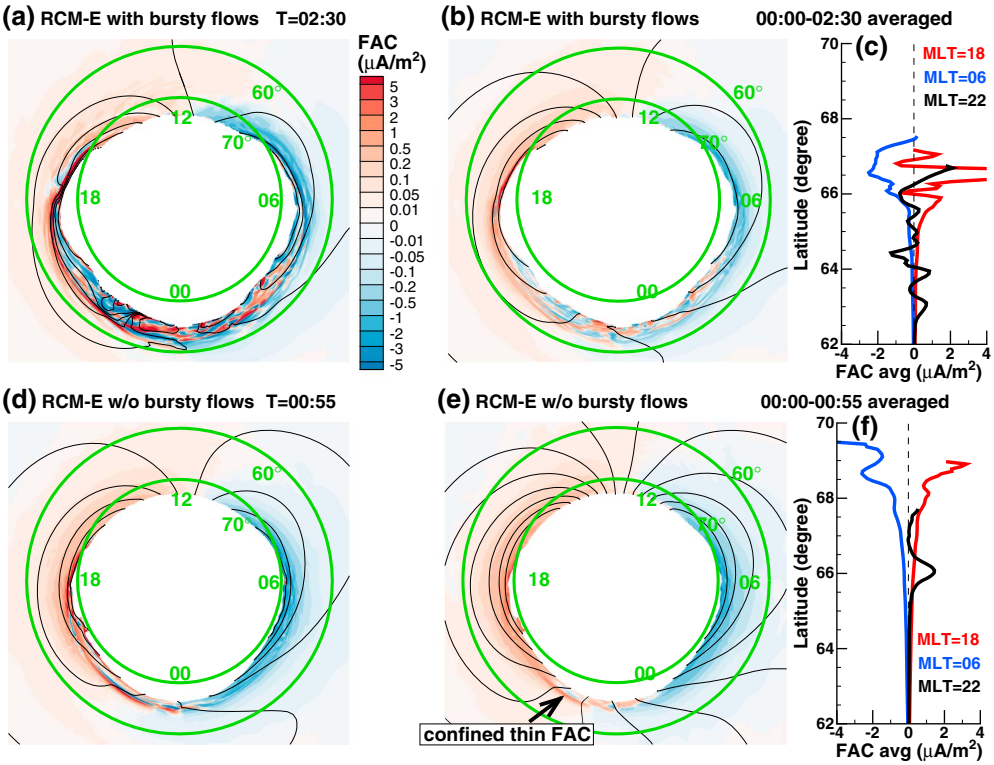

Figure 3. Ionospheric view of simulated field-aligned current (FAC) densities ((a), (b), (d), and (e)) with red being downward and blue being upward. Black lines are electric equipotentials every 5 kV. Average FAC density profiles along colatitudes at three different local times ((c) and (f)).

simulations can explicitly reveal the importance of intermittent bursty flows in the average configurations of the plasma sheet and the ionosphere.

The most important result of the study is that when we assume bubbles and blobs flowing through the RCM tailward boundary at a level consistent with Geotail data, the simulation produces a tailward gradient of $PV^{5/3}$ in the central plasma sheet that is more consistent with statistical results than any simulations we have carried out without bubbles.

A relevant issue is the distribution of FACs that is associated with the gradient of $PV^{5/3}$ in equilibrium conditions. Over the decades, the RCM has tended to predict region 2 currents, which are associated with the inner edge of the plasma sheet, to be thinner in latitude than is typically observed [*Harel et al.*, 1981]. The same is true for the no-bursty-flow run (bottom panel of Figure 3), which only exhibits a substantial gradient of $PV^{5/3}$ from about 7 to 12 Re. The discrepancy is resolved for the run with bursty flows (top panel of Figure 3). The simulation with bursty flows not only resolves the aforementioned inconsistencies between theory and data but also preserves the features that have been well predicted by previous RCM simulations, i.e., the region 2 FACs in the classic *Iijima and Potemra* [1978] diagram and the classic two-cell convection picture in the closed-field-line region.

It is worth noting that the simulation in the absence of bursty flows results in a continuously stretching tail magnetic field. Eventually, the code fails to find a physical solution. Presumably in nature, the continuous decrease of B_Z in the central plasma sheet will eventually give rise to small-scale instabilities that violate the adiabatic-drift conditions and initiate substorm expansion. In that sense, nature opts to resolve the pressure balance inconsistency accumulated in the substorm growth phase in an explosive way. This suggests that adiabatic earthward convection of fully populated flux tubes is unlikely to last for many hours. However, we have noticed that both empirical modeling [*Stephens et al.*, 2013] and other RCM-E simulations [*Yang et al.*, 2012] suggest that the inconsistency can also be resolved for Steady Magnetospheric Convection events, if $PV^{5/3}$ at ~20 R_E is relatively small.

The simulations presented in this paper can and will be improved in several aspects in the future. (1) More computer experiments will be needed to determine the sensitivity of the results to various input parameters (e.g., average level and MLT dependence of $PV^{5/3}$, magnitude of the $PV^{5/3}$ depletion inside bubbles, plasma-sheet temperature). (2) We have assumed that the bubbles/blobs are created through non-adiabatic processes tailward of ~20 R_E. However, the discrepancy in $PV^{5/3}$ inside 14 Re encourages us to explore the effects of violation of adiabaticity inside RCM-E simulation region. (3) The RCM-E simulations need to include inertial effects, which are crucial for accurate calculation of the motion of bubbles (e.g., overshoot/braking phenomenon) and associated FACs. Based on our calculation of average sound wave speed in the plasma sheet and the interchange oscillation period of a bubble [*Wolf et al.*, 2012a], we conclude that a bubble with an average injection speed greater than 300 km/s will substantially violate the RCM-E slow-flow approximation. However, because the neglect of inertial effects can lead to artificially high velocities for a given reduction in $PV^{5/3}$ [*Wolf et al.*, 2012b], we anticipate that when we include inertia, more severely depleted bubbles will have to be introduced in the simulation to maintain the same degree of agreement in V_X PDF. We thus expect the agreement in the $PV^{5/3}$ profile to be improved. (4) The RCM-E simulations need to include effects of field-aligned potential drops, which are now assumed to be zero. (5) We have to verify whether the predicted degree of bubble/blob-associated irregularity in simulated Birkeland currents is consistent with variability in observations. However, the initial results presented here, although with notable theoretical limitations, have moved a pivotal step toward understanding how the non-adiabatic microphysics that can give rise to bubbles and blobs can affect the large-scale plasma sheet structure and M-I coupling in a statistical way, through meso-scale transport.

Acknowledgments

We would like to thank Timothy Guild and Mikhail Sitnov for useful discussions. The work was partially motivated by conservations with Richard L. Kaufmann (UNH). The work at Rice was supported by NASA Heliophysics Theory grant NNX11AJ38G, NASA Guest Investigator grant NNX10AQ43G, and NASA LWS TR&T NNX13AF92G. The work at UCLA was supported by NASA NNX11AJ12G and NSF ATM-1003595. We thank T. Mukai at ISAS and CDAWeb for the use of the Geotail LEP data. The Geotail magnetic field data were provided through the DARTS system by ISAS. We thank Jon Vandegriff of the Applied Physics Laboratory for providing the Geotail EPIC data.

The Editor thanks two anonymous reviewers for their assistance in evaluating this paper.

References

Angelopoulos, V., et al. (1994), Statistical characteristics of bursty bulk flow events, *J. Geophys. Res.*, *99*, 21,257–21,280.

Angelopoulos, V., T. Mukai, and S. Kokubun (1999), Evidence of intermittency in Earth's plasma sheet and implications for self-organized criticality, *Phys. Plasmas*, *6*, 4161.

Birn, J., J. Raeder, Y. L. Wang, R. A. Wolf, and M. Hesse (2004), On the propagation of bubbles in the geomagnetic tail, *Ann. Geophys.*, *22*, 1773–1786.

Borovsky, J. E., R. C. Elphic, H. O. Funsten, and M. F. Thomsen (1997), The Earth's plasma sheet as a laboratory for flow turbulence in high-beta MHD, *J. Plasma Phys.*, *57*, 1.

Erickson, G. M., and R. A. Wolf (1980), Is steady convection possible in the Earth's magnetotail?, *Geophys. Res. Lett.*, *7*, 897–900.

Guild, T. B., H. E. Spence, E. L. Kepko, V. Merkin, J. G. Lyon, M. Wiltberger, and C. C. Goodrich (2008), Geotail and LFM comparisons of plasma sheet climatology: 2. Flow variability, *J. Geophys. Res.*, *113*, A04217, doi:10.1029/2007JA012613.

Harel, M., R. A. Wolf, R. W. Spiro, P. H. Reiff, C.-K. Chen, W. J. Burke, F. J. Rich, and M. Smiddy (1981), Quantitative simulation of a magnetospheric substorm 2. Comparison with observations, *J. Geophys. Res.*, *86*(A4), 2242–2260, doi:10.1029/JA086iA04p02242.

Hsu, T.-S., R. L. McPherron, V. Angelopoulos, Y. Ge, H. Zhang, C. Russell, X. Chu, and J. Kissinger (2012), A statistical analysis of the association between fast plasma flows and Pi2 pulsations, *J. Geophys. Res.*, *117*, A11221, doi:10.1029/2012JA018173.

Iijima, T., and T. A. Potemra (1978), Large-scale characteristics of field-aligned currents associated with substorms, *J. Geophys. Res.*, *83*(A2), 599–615, doi:10.1029/JA083iA02p00599.

Kaufmann, R. L., W. R. Paterson, and L. A. Frank (2004), Pressure, volume, density relationships in the plasma sheet, *J. Geophys. Res.*, *109*, A08204, doi:10.1029/2003JA010317.

Lemon, C., F. R. Toffoletto, M. Hesse, and J. Birn (2003), Computing magnetospheric force equilibria, *J. Geophys. Res.*, *108*(A6), 1237, doi:10.1029/2002JA009702.

Nakamura, R., et al. (2004), Spatial scale of high-speed flows in the plasma sheet observed by Cluster, *Geophys. Res. Lett.*, *31*, L09804, doi:10.1029/2004GL019558.

Pontius, D. H., Jr., and R. A. Wolf (1990), Transient flux tubes in the terrestrial magnetosphere, *Geophys. Res. Lett.*, *17*(1), 49–52, doi:10.1029/GL017i001p00049.

Runov, A., V. Angelopoulos, and X.-Z. Zhou (2012), Multipoint observations of dipolarization front formation by magnetotail reconnection, *J. Geophys. Res.*, *117*, A05230, doi:10.1029/2011JA017361.

Sergeev, V. A., V. Angelopoulos, J. T. Gosling, C. A. Cattell, and C. T. Russell (1996), Detection of localized, plasma-depleted flux tubes or bubbles in the midtail plasma sheet, *J. Geophys. Res.*, *101*(A5), 10,817–10,826.

Stephens, G. K., M. I. Sitnov, J. Kissinger, N. A. Tsyganenko, R. L. McPherron, H. Korth, and B. J. Anderson (2013), Empirical reconstruction of storm time steady magnetospheric convection events, *J. Geophys. Res. Space Physics*, *118*, 6434–6456, doi:10.1002/jgra.50592.

Toffoletto, F. R., S. Sazykin, R. Spiro, and R. Wolf (2003), Inner magnetospheric modeling with the Rice Convection Model, *Space Sci. Rev.*, *107*, 175–196, doi:10.1023/A:1025532008047.

Tsyganenko, N. A. (1989), Magnetospheric magnetic field model with a warped tail current sheet, *Planet. Space Sci.*, *37*, 5–20, doi:10.1016/0032-0633(89)90066-4.

Wolf, R. A., Y. Wan, X. Xing, J.-C. Zhang, and S. Sazykin (2009), Entropy and plasma sheet transport, *J. Geophys. Res.*, *114*, A00D05, doi:10.1029/2009JA014044.

Wolf, R. A., C. X. Chen, and F. R. Toffoletto (2012a), Thin-filament simulations for Earth's plasma sheet: Interchange oscillations, *J. Geophys. Res.*, *117*, A02215, doi:10.1029/2011ja016971.

Wolf, R. A., C. X. Chen, and F. R. Toffoletto (2012b), Thin filament simulations for Earth's plasma sheet: Tests of validity of the quasi-static convection approximation, *J. Geophys. Res.*, *117*, A02216, doi:10.1029/2011JA016972.

Xing, X., and R. A. Wolf (2007), Criterion for interchange instability in a plasma connected to a conducting ionosphere, *J. Geophys. Res.*, *112* , A12209, doi:10.1029/2007JA012535.

Yang, J., F. R. Toffoletto, X. Xing, and V. Angelopoulos (2012), RCM-E simulation of the 13 March 2009 steady magnetospheric convection event, *J. Geophys. Res.*, *117*, A03224, doi:10.1029/2011JA017245.